

## ARTICLE

# PCL/ $\beta$ -AgVO<sub>3</sub> nanocomposites obtained by solvent casting as potential antimicrobial biomaterials

Beatriz Rossi Canuto de Menezes<sup>1</sup>  | Thaís Larissa do Amaral Montanheiro<sup>1,2</sup>  |  
 Aline da Graça Sampaio<sup>3</sup>  | Cristiane Yumi Koga-Ito<sup>3</sup>  |  
 Gilmar Patrocínio Thim<sup>1</sup>  | Larissa Stieven Montagna<sup>2</sup> 

<sup>1</sup>Laboratory of Plasmas and Processes, Technological Institute of Aeronautics, São Paulo, Brazil

<sup>2</sup>Technology Laboratory of Polymers and Biopolymers, Federal University of São Paulo, São Paulo, Brazil

<sup>3</sup>Genoma Laboratory, São José dos Campos Institute of Science and Technology, São Paulo State University (UNESP), São Paulo, Brazil

## Correspondence

Beatriz Rossi Canuto de Menezes, Laboratory of Plasmas and Processes, Technological Institute of Aeronautics, Praça Marechal Eduardo Gomes, 50-Vila das Acácias, São José dos Campos, São Paulo 12228-900, Brazil  
 Email: beatriz1menezes@gmail.com

## Funding information

Coordenação de Aperfeiçoamento de Pessoal de Nível Superior, Grant/Award Number: n/a; Financiadora de Estudos e Projetos, Grant/Award Number: 01.13.0328.03; Fundação de Amparo à Pesquisa do Estado de São Paulo (BR), Grant/Award Numbers: 2017/24873-4, 2017/02846-5; Fundação de Amparo à Pesquisa do Estado de São Paulo, Grant/Award Number: 2018/12035-7

## Abstract

The adhesion of microorganisms on biomaterials can impair its effective application. The addition of antimicrobial agents is a promising alternative to overcome this limitation. In this work, films of polycaprolactone (PCL) and nanostructured  $\beta$ -AgVO<sub>3</sub> (SV) were produced by solvent casting with 0.1, 0.5, and 1.0 wt% of SV. The effect of SV on the structure of PCL was investigated using Fourier transform infrared spectroscopy (FTIR), X-ray diffraction (XRD), Raman spectroscopy, differential scanning calorimetry (DSC), and scanning electron microscopy (SEM). The antimicrobial activity of the films against *Staphylococcus aureus* and *Escherichia coli* was evaluated by the agar diffusion method and by direct contact test. FTIR confirmed the presence of SV into the PCL films, with chemical interaction between them. SEM showed that SV nanorods were well dispersed and with good interfacial adhesion with PCL. XRD diffraction and Raman spectroscopy showed that the presence of SV increased the number of nucleation sites, reducing the size of crystallites and increasing the amorphous domains in the PCL matrix, consequently reducing crystallinity. This behavior was confirmed by DSC, which showed a reduction in the crystallinity with increasing SV content. Films with 1 wt% of SV showed antimicrobial activity against *Staphylococcus aureus* in direct contact test.

## KEYWORDS

biocompatibility, biomedical applications, films, nanoparticles, nanowires and nanocrystals

## 1 | INTRODUCTION

The development and research of innovative biomaterials with antimicrobial properties, biocompatible, and non-toxic have attracted interest from the scientific community for application in the biomedical and dental products.<sup>1</sup> Moreover, antimicrobial properties are highly desirable in products and equipment intended for biomedical and dental applications, due to the tendency of

microbial proliferation on the materials contact surface and the tissue formation region, in the case of scaffolds.<sup>2-4</sup>

Polycaprolactone (PCL) is a synthetic, flexible, biodegradable, biocompatible, and hydrophobic aliphatic polyester.<sup>5-9</sup> Furthermore, PCL has a cost-efficient perspective, good processability, low melting temperature (~60°C), and also takes a very long time to degrade compared with other biopolymers, like poly(lactic acid)

(PLA), and polyhydroxyalkanoates (PHA) family.<sup>10,11</sup> For this reason, it is one of the most widely used biopolymers in the medical and dental areas, as scaffolds in tissue engineering and cartilage, fibers for guided bone regeneration, in the use of medical implants, sutures, dressings and in the drug distribution control system, and in the environmental area, as ecologically friendly biodegradable plastics.<sup>7,9,12–16</sup>

However, biopolymers have certain undesirable properties when biomedical and dental applications are intended, as insufficient mechanical properties, lack of bioactivity, and low antimicrobial activity.<sup>17,18</sup> In this way, it is necessary to modify the biopolymer to improve the thermal, mechanical properties, cell adhesion potential, cell proliferation, and antimicrobial properties. One way would be by incorporating nanoparticles, such as, silver vanadate ( $\text{AgVO}_3$ ), in the biopolymer matrix during the processing.<sup>19–21</sup>

$\text{AgVO}_3$  is a nanoparticle that presents low toxicity to human cells, excellent antimicrobial activity, and shows several applications, such as, sensors, batteries, photocatalyst, and antimicrobial agent, especially in the biomedical field; besides being considered the most common form of the solid-state silver vanadate oxides.<sup>22–26</sup> The crystalline  $\text{AgVO}_3$  have four different polymorphs in its crystallography, alpha ( $\alpha$ ), beta ( $\beta$ ), gamma ( $\gamma$ ), and delta ( $\delta$ ), but the more commons are alpha and beta.<sup>22,27</sup>  $\beta\text{-AgVO}_3$  presents a monoclinic space group and is thermodynamically stable with considerable antibacterial activity, especially due to the silver nanoparticles (AgNPs) that precipitated in its surfaces.  $\alpha\text{-AgVO}_3$  is a metastable phase, and little is known about its antimicrobial properties.<sup>24</sup>

$\beta\text{-AgVO}_3$  nanoparticle has shown promising antimicrobial activity on Gram-positive bacteria (*Staphylococcus aureus*<sup>21</sup> and *Enterococcus faecalis*), Gram-negative bacteria (*Escherichia coli*<sup>28</sup> and *Pseudomonas aeruginosa*) and fungi (*Candida albicans*<sup>29</sup>), reaching a broad spectrum of antimicrobial action.  $\beta\text{-AgVO}_3$  has shown antimicrobial potential in dental resin<sup>30</sup> due to the ability to act on the surface of bacteria, which may vary according to the shape, size, and surface charge of the particle.<sup>30</sup>

There are a limited number of researchers that have reported the improvement in antimicrobial property with the addition of  $\beta\text{-AgVO}_3$  in the polymer matrix, one of them is the research conducted by Castro et al.<sup>20</sup> The authors incorporated concentrations of 0.5, 1, 2.5, 5, and 10 wt% of  $\beta\text{-AgVO}_3$  in dental acrylic resins (poly(methyl methacrylate) (PMMA), and verified the influence of these nanoparticles on the antimicrobial (metabolic activity of *C. albicans* and *Streptococcus mutans*) and mechanical properties. As the results, incorporation of 10 wt%  $\beta\text{-AgVO}_3$  significantly reduced the microbial metabolic

activity. The nanoparticle did not change the mechanical properties of hardness and surface roughness of the resins but caused a decrease in flexural strength with the addition of amounts greater than 1 wt%.

*S. aureus* and *E. coli* are some of the main microorganism that affect biomaterials, reducing their performance and resulting in serious injuries for the patients. *S. aureus* is a pathogenic microorganism capable of causing a broad range of clinical infections, especially related to foreign bodies, as prostheses used as cardiac valves, joints, intravascular catheters, breast implants, and scaffolds, among others.<sup>31</sup> The formation of *S. aureus* biofilm on biomaterials results in severe infections and may cause the failure of implants and prostheses.<sup>32</sup> *E. coli* is also a pathogenic microorganism that can be commonly transmitted in hospitals and cause most of urinary catheters infections.<sup>33,34</sup>

The adhesion of microorganism in prostheses and implants surfaces competes with the cell integration, impairing the biological effect desired. Besides, infections caused by microorganism can results in the failure of the biomaterial.<sup>35</sup> In order to minimize and avoid the problems caused by microorganism, antimicrobial agents, such as,  $\beta\text{-AgVO}_3$ , have been added into biomaterials. Although PCL has already been used as biomaterials, such as, scaffolds,<sup>36</sup> membranes,<sup>37</sup> catheter,<sup>38</sup> joint regeneration,<sup>39</sup> among others, this polymer still presents complications related to microorganism adhesion. To the best of our knowledge, it is the first time that  $\beta\text{-AgVO}_3$  is incorporated into PCL matrix. In this way, this work studied the influence of  $\beta\text{-AgVO}_3$  on the chemical, thermal properties, morphological characteristics, and antimicrobial properties of PCL to obtain bionanomaterials with desirable properties for application as prostheses and implants, in the dental and biomedical products.

## 2 | EXPERIMENTAL

### 2.1 | $\beta\text{-AgVO}_3$ synthesis

Nanostructured  $\beta\text{-AgVO}_3$ , labeled as SV, was synthesized through a hydrothermal process, according to the methodology proposed by de Menezes et al.<sup>22</sup> Initially, 0.7197 g of silver nitrate ( $\text{AgNO}_3$ ) (Neon, 99%, Brazil) and 0.5109 g of ammonium metavanadate ( $\text{NH}_4\text{VO}_3$ ) (Neon, 99%, Brazil) were separately dissolved in 50 ml of deionized water. The two obtained aqueous solutions were mixed and stirred for 10 min at room temperature. Then, the final solution was transferred into a 200 ml Teflon-lined stainless-steel autoclave, which was heated at 180°C and maintained for 8 h in an oven. The product was filtered and washed with deionized water and

absolute ethyl alcohol (C<sub>2</sub>H<sub>6</sub>O) (Neon, 95%, Brazil). Finally, the material was dried in conventional oven at 60°C for 12 h.

## 2.2 | PCL/SV nanocomposite films

PCL/SV nanocomposite films were prepared by solvent casting, according to the methodology described by Montagna et al.<sup>40</sup> and Montanheiro et al.<sup>41</sup> SV (0.0, 0.1, 0.5, and 1.0 wt%) and chloroform (CHCl<sub>3</sub>) (Synth, 100%, Brazil).

(1:10 wt/v) were sonicated for 4 min in a Sonics Vibra Cell (VC750, 20 Hz) ultrasonic processor with 25% of amplitude. Then, PCL (Sigma–Aldrich, Saint Louis) with density of 1.145 g/cm<sup>3</sup> and *M<sub>w</sub>* equal to 80,000 g/mol, was solubilized in chloroform (1.1:10wt/v) at 30°C under stirring until the entire polymer mass has been dissolved and resulted in a viscous solution. Subsequently, the solution containing the SV was stirred with the PCL solution and sonicated again for 2 min. The final solution was cast onto Petri dishes covered with aluminum foil to obtain films after solvent evaporation at room temperature for 6 h. Samples were labeled according to Table 1.

## 2.3 | Characterization

### 2.3.1 | Fourier transform infrared spectroscopy (FTIR)

SV and the nanocomposites were characterized by Fourier-transformed infrared (FTIR) spectroscopy in a PerkinElmer Spectrum One equipment, using universal attenuated total reflectance (UATR) from 400 to 4000 cm<sup>-1</sup>.

### 2.3.2 | X-ray diffraction (XRD)

XRD analysis was performed in a PANalytical Philips X'Pert diffractometer operating with CuK $\alpha$  radiation ( $\lambda = 1.54178 \text{ \AA}$ ) at 45 kV and 40 mA. The data were collected using transmission technique, in the  $2\theta$  range from

10° to 50°, at room temperature, with step size of 0.02°, and 30 s per step. The crystallite size (*C*) was calculated for the main peak with highest intensity (100) by Scherrer's equation (Equation 1):

$$C = \frac{0.9\lambda}{\beta \cos\theta} \quad (1)$$

where  $\lambda$  is the wavelength of Cu radiation (0.154 nm),  $\beta$  is the width at half height in nanometers, and  $\theta$  is the Bragg angle in the plan related to the peak. The width at half height was obtained by the following equation (Equation 2):

$$\beta = \frac{\rho 2\pi}{360} \quad (2)$$

where  $\rho$  is the half-height width of the peak (FWHM).<sup>42</sup> The crystallinity degree (*X<sub>c</sub>*) of the neat PCL and nanocomposites was calculated by the crystalline and noncrystalline areas (Equation 3):

$$X_c = \frac{I_c}{I_c + I_a} \quad (3)$$

where *I<sub>c</sub>* is the area of crystalline peaks and *I<sub>a</sub>* is the area of noncrystalline peaks.<sup>43</sup>

### 2.3.3 | Raman spectroscopy

Raman spectroscopy of neat PCL and PCL/SV nanocomposites was performed in a Horiba LabRam HR Evolution equipment excited in the visible range with an Ar laser with 532 nm. A research grade Leica DM LM microscope with objective magnification of 100 $\times$  was used to focus the laser beam on the sample. The analysis was performed between 200 and 1800 cm<sup>-1</sup>, with laser filter of 25%, cumulative acquisition time of 60 s and 3 accumulations.

### 2.3.4 | Differential scanning calorimetry (DSC)

DSC analyses of neat PCL and PCL/SV nanocomposites were performed on a Netzsch Phoenix DSC 2014 F1. Small amounts (10 mg) of dried samples were placed into aluminum pans. Samples were heated at a heating rate of 10°C/min from 25 to 200°C, in a N<sub>2</sub> atmosphere with a gas flow of 20 ml/min, to eliminate the heat history. Subsequently, samples were cooled to 0 at 10°C/min, to obtain the crystallization temperature (*T<sub>c</sub>*). After that,

**TABLE 1** Composition and nomenclature of samples

Composition	Nomenclature
Neat PCL	PCL
PCL/0.1 wt% $\beta$ -AgVO <sub>3</sub>	PCL/0.1SV
PCL/0.5 wt% $\beta$ -AgVO <sub>3</sub>	PCL/0.5SV
PCL/1.0 wt% $\beta$ -AgVO <sub>3</sub>	PCL/1.0SV

they were heated to 250°C at 10°C/min, to obtain the melting point ( $T_m$ ) and the melting enthalpy ( $\Delta H_m$ ). The degree of crystallinity ( $X_c$ ) of the samples was determined by the following equation (Equation 4):

$$X_c(\%) = \left( \frac{\Delta H_m}{\Delta H_m^0} \right) \times \Phi_{PCL} \times 100 \quad (4)$$

where  $\Delta H_m$  is the melting enthalpy obtained by DSC,  $\Delta H_m^0$  is the theoretical melting heat value for 100% crystalline PCL, which was taken as 132 J/g,<sup>44</sup> and  $\Phi_{PCL}$  is the mass fraction of PCL in the nanocomposites.

### 2.3.5 | Transmission (TEM) and scanning electron microscopy (SEM)

SV morphology was observed in a transmission electron microscopy (TEM) using a JEM 2100–JEOL and Field Emission Gun–Scanning electron microscopy (FEG–SEM) using a MIRA3–TESCAN.

The morphological surface of PCL and PCL/SV nanocomposites was observed by SEM using an Inspect S50–FEI Company<sup>®</sup> microscope, with detectors of secondary electrons mode (SE) and an accelerating voltage of 7.5 kV. The samples were fixed on aluminum stubs and covered with gold.

The cryogenic fracture surface morphology of PCL and PCL/SV nanocomposites was analyzed by Field Emission Gun–Scanning Electron Microscopy (FEG–SEM) using a MIRA3–TESCAN. The samples were cryogenically fractured, fixed on aluminum stubs, and covered with gold.

### 2.3.6 | Antimicrobial activity assessment by agar diffusion method

The antimicrobial activity of PCL and PCL/SV nanocomposites was evaluated using the agar diffusion method, according to CLSI (Clinical and Laboratory Standards Institute).<sup>45</sup> *Staphylococcus aureus* (ATCC 6538, Gram-positive bacterium) and *Escherichia coli* (ATCC 10799, Gram-negative bacterium) were plated on brain heart infusion (BHI) agar and plates were incubated at 37°C for 24 h, under aerobiosis. PCL and PCL/SV film discs (33.4 mm<sup>2</sup>) were sterilized by exposition to UV light (ultra-violet) for 10 min per side. Sterility testing was performed to prove the efficacy of the procedure, by using both liquid and solid culture media.

The sample groups tested were neat PCL, PCL/0.1SV, PCL/0.5SV, and PCL/1.0SV. Standardized suspensions

(10<sup>6</sup> cells.ml<sup>-1</sup>) were prepared in saline solution (NaCl 0.9%) with the aid of a spectrophotometer (AJX-1600, AJMICRONAL) (*S. aureus* wavelength 490 nm; absorbance 0.029; *E. coli* wavelength of 600 nm, absorbance of 0.005). Aliquots of 100 µl of the suspension were plated, with the aid of a sterile swab, on the surface of the Mueller-Hinton agar. Plates were left open under aseptic conditions for 10 min, for drying. Subsequently, three sterile specimens were distributed at equidistant points on the culture medium and incubated at 37°C for 24 h. After the period of incubation, the formation of the zone of inhibition was analyzed. This assay was carried out in triplicate on in three different occasions (n = 9/group).

### 2.3.7 | Antimicrobial activity assessment by direct contact test

The antibacterial activity was also tested in a direct contact test. The sample groups tested were neat PCL, PCL/0.1SV, PCL/0.5SV, and PCL/1.0SV. The specimens were sterilized as described above. Standardized bacterial suspension of *S. aureus* and *E. coli* at a concentration of 10<sup>6</sup> cells/mL was obtained. For direct contact test, the specimens were immersed individually in microtubes containing 900 µl of BHI broth and, after, 100 µl of the bacterial suspension was added. The tubes were incubated at 37°C for 24 h, under aerobiosis. Thereafter, successive serial dilutions were obtained and plated on BHI agar. Plates were incubated at 37°C for 24 h, under aerobiosis. Subsequently, the number of colony-forming units per milliliter (CFU ml<sup>-1</sup>) was determined. A negative control group, without any sample of PCL or PCL/SV nanocomposite specimen, was included in the experiments. This assay was carried out in triplicate on in three different occasions (n = 9/group). The bacterial reduction percent (R%) was determined according to Equation 5:

$$R(\%) = ([B - A]/A) \times 100 \quad (5)$$

where B is the mean number of bacterial colonies (CFU ml<sup>-1</sup>) observed in the control and A is the mean number of bacterial colonies (CFU ml<sup>-1</sup>) after contact with PCL/SV nanocomposites.<sup>46</sup>

### 2.3.8 | Data analysis

The normal distribution of data was verified by Shapiro-Wilks test. Data were compared by One-way ANOVA and Dunnett's multiple comparison test. The level of significance of 5% was adopted. The software used was GraphPad Prism v 7.0.



### 3 | RESULTS

#### 3.1 | Fourier transform infrared spectroscopy (FTIR)

FTIR measurements were conducted to evaluate the changes on PCL matrix produced by the SV nanorods incorporation. Figure 1(a) shows the FTIR analyses of SV, PCL, and PCL/SV nanocomposites with 0.1, 0.5, and 1.0 wt% of SV. Neat SV presents two main bands, located at 774 and 457  $\text{cm}^{-1}$ , attributed to V—O vibrations.<sup>21</sup> PCL shows main bands located at 2947 and 2863  $\text{cm}^{-1}$ , attributed to C—H vibrations, 1717  $\text{cm}^{-1}$  attributed to C=O vibrations<sup>47</sup> and at 1168  $\text{cm}^{-1}$  due to C—O stretching.<sup>48</sup>

The composites have the same characteristic bands as the neat PCL; however, a new absorption band could be observed at about 502  $\text{cm}^{-1}$ , which intensity became stronger with increasing SV content in PCL. The presence of this new band not only confirms the presence of SV into PCL composites but also might indicate an interaction between PCL and the V—O bonds in the SV surface, due to the shift in the band wavelength.<sup>49,50</sup>

Interaction between the polymer matrix and the nanoparticle is an important key to obtain improved composite properties, such as, mechanical, thermal, and rheological.<sup>51–55</sup> Polymer-filler interfacial interactions are intermolecular interactions that occur between the polymer chains and the filler, such as, hydrogen bonding and van der Waals forces, for example, which are generated by the transient or permanent dipoles of the molecules.<sup>52,56–59</sup> In some cases, surface modifications of fillers are necessary to obtain effective dispersion and interaction with the matrix. Weak interfacial interaction

may be resultant from differences in polarity between the filler and the matrix, for example.<sup>60</sup> Well dispersed nanoparticles may also be responsible for strong matrix-filler interactions.<sup>61</sup>

#### 3.2 | Raman spectroscopy

Figure 1(b) displays the Raman spectra of SV, neat PCL, and its nanocomposites. Raman spectroscopy is an important nondestructive technique used to characterize the microstructure of several materials. Concerning SV, characteristic bands were observed, being the most intense at 884  $\text{cm}^{-1}$ , related to stretching vibrations of V—O—Ag, Ag—O—Ag, and O—V—O.<sup>62</sup> The band at 840  $\text{cm}^{-1}$  is associated to stretching vibrations of V—O groups in  $(\text{V}_2\text{O}_7)^{4-}$  ion and Ag—O—V stretching vibrations.<sup>62</sup> Ag—O—Ag bridges stretching vibrations are assigned to the band at 805  $\text{cm}^{-1}$ , while  $\text{VO}_4$  deformation mode is associated with the band at 728  $\text{cm}^{-1}$ .<sup>62</sup> Raman band at 515  $\text{cm}^{-1}$  is attributed to asymmetric stretching of V—O—V in the polymeric chains of metavanadate.<sup>62</sup> The asymmetric deformation of  $\text{VO}_4^{3-}$  tetrahedron is associated with the bands at 384 and 334  $\text{cm}^{-1}$ .<sup>62</sup> The bands at 271 and 243  $\text{cm}^{-1}$  are associated with asymmetrical and symmetrical folding of  $\text{VO}_4^{3-}$  tetrahedron, respectively.<sup>62</sup>

The characteristic bands of PCL were also observed. The narrow band at 1720  $\text{cm}^{-1}$  is related to C=O stretching mode.<sup>63,64</sup> The group of bands at 1470, 1440, and 1415  $\text{cm}^{-1}$  are associated with  $\text{CH}_2$  groups scissor vibration, while the bands at 1300 and 1280  $\text{cm}^{-1}$  are assigned to  $\text{CH}_2$  groups wagging vibration.<sup>63,64</sup> The bands

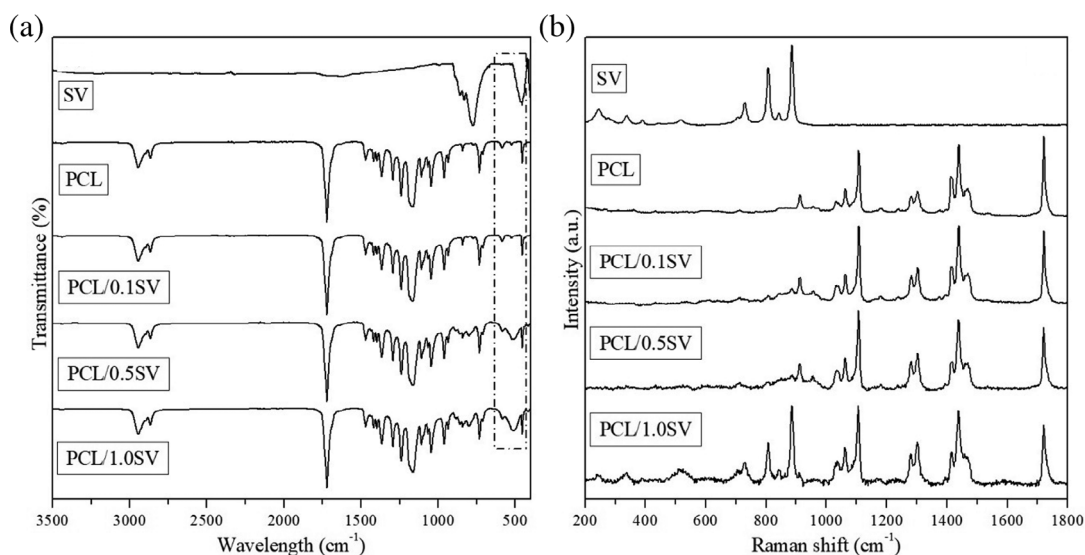


**FIGURE 1** (a) Fourier transform infrared spectra and (b) Raman spectra of SV, PCL, PCL/0.1SV, PCL/0.5SV, and PCL/1.0SV

at 1108, 1065, and 1030  $\text{cm}^{-1}$  are related to C—O—C stretching vibrations, and the band at 912  $\text{cm}^{-1}$  is attributed to C—COO scissoring.<sup>63,64</sup> All the observed bands are relatively narrow and intense, indicating the presence of crystalline domains for neat PCL. The absence of bands related to amorphous domains, as the band at 850  $\text{cm}^{-1}$  (C—COO scissoring), 1097  $\text{cm}^{-1}$  (C—O—C stretching), and 1733  $\text{cm}^{-1}$  (C=O stretching), leads the conclusion that the PCL films are highly crystalline.<sup>64</sup>

Regarding the PCL/SV nanocomposites, the characteristic bands of PCL and the most intense bands of SV (884  $\text{cm}^{-1}$ ) can be observed. Thus, both PCL and SV did not suffer any modification in composition during the fabrication process of nanocomposites.<sup>65</sup> However, the widening of the band at 1720  $\text{cm}^{-1}$ , measured by the full width at half height (FWHM), can be observed after the incorporation of SV, when compared with the neat PCL (Table 2).

The addition of higher amounts of SV resulted in wider bands. Compared with neat PCL, the addition of 0.1% of SV increased the FWHM in about 13%, while the incorporation of 1.0% of SV increased the FWHM in about 64%. Usually, the widening of Raman bands in semi-crystalline materials is associated with the growth of amorphous domains, reducing the polymer crystallinity.<sup>64</sup>

Similar results were found by Kołodziej et al.<sup>64</sup> The authors reported an increase in the FWHM of the band at 1720  $\text{cm}^{-1}$  after the incorporation of multi-walled carbon nanotubes (MWCNTs) in PCL. The results were associated with the reduction of material crystallinity due to the growth of amorphous domains.

According to the Raman results, the incorporation of SV in PCL significantly affected the PCL molecular chain, reducing the crystallinity.

### 3.3 | X-ray diffraction (XRD)

XRD measurements were performed to characterize the crystalline structure of neat PCL and nanocomposites and verify if the SV incorporation interferes in the basic crystalline structure of PCL. Figure 2 shows the XRD

patterns of SV, neat PCL and its nanocomposites with 0.1, 0.5, and 1.0 wt% of SV. SV (Figure 2(a)) showed diffraction peaks attributed to the monoclinic  $\beta\text{-AgVO}_3$  phase with Joint Committee on Power Diffraction Standards (JCPDS) 29-1154.<sup>22</sup> Neat PCL and nanocomposites (Figure 2(b)) exhibited diffraction peaks indexed to the orthorhombic space group,  $P2_12_12_1-D_2^4$ , which is the characteristic crystalline structure of PCL.<sup>66,67</sup> Two distinct diffraction peaks are verified for all samples at around  $2\theta = 21.4^\circ$  and  $23.8^\circ$ , corresponding to the (110), and (200) planes, respectively.<sup>68</sup> A small shoulder at around  $2\theta = 22.2^\circ$  can also be observed and is related to the plane (111).<sup>69</sup>

The position of these peaks remains substantially unchanged when PCL is compared with the nanocomposites, indicating that the incorporation of SV, in any concentration, does not affect the basic crystalline structure of PCL.<sup>70</sup> Also, very small peaks at around  $28.5$  and  $30.0^\circ$  can be observed for the nanocomposites, especially the PCL/1.0SV, which are attributed to SV most intense peaks and indicate the presence of SV in the nanocomposites.

Table 3 presents the calculated crystallite size for (100) plane, crystallinity degree ( $X_c$ ), and lattice parameters for neat PCL and nanocomposites. The sizes of crystallite for all samples were very similar. Usually, the crystallite size of polymers tends to reduce after the incorporation of nanofiller.<sup>55</sup> However, in this case, only a slight reduction was observed after the incorporation of SV nanorods, indicating that the nanomaterials have no effect on this parameter. The calculated lattice parameters for neat PCL was  $a = 6.7 \text{ \AA}$ ,  $b = 5.3 \text{ \AA}$ , and  $c = 16.1 \text{ \AA}$ , similar to those found in the literature.<sup>66</sup> The nanocomposites showed similar lattice parameters, indicating that no reaction or atomic replacement between PCL and SV nanorods happen.

As mentioned in FTIR discussion, the interaction between polymer matrices and nanofillers happen through intermolecular interactions, such as, van der Waals forces that are generated by transient or permanent dipoles.<sup>52,56-59</sup> In this way, the addition of nanofillers in PCL will not interfere in the short range arrangement of the polymeric structure.<sup>71</sup> The results of crystallite size and lattice parameters confirms that the incorporation of SV, in any concentration, does not affect the basic crystalline structure of PCL.

A reduction in the crystallinity degree was observed for the nanocomposites, being 5.5%, 9.0%, and 13.6% for PCL/0.1SV, PCL/0.5SV, and PCL/1.0SV, respectively, compared with neat PCL. SV nanoparticles can act in the two main mechanism of crystallization: nucleation and growth. The presence of nanomaterials in a polymeric matrix induces the formation of more nucleation sites,

**TABLE 2** Calculated full width at half height (FWHM) of neat PCL and nanocomposites, concerning the band at 1720  $\text{cm}^{-1}$

Sample	FWHM
PCL	8.3
PCL/0.1SV	9.4
PCL/0.5SV	11.1
PCL/1.0SV	13.6

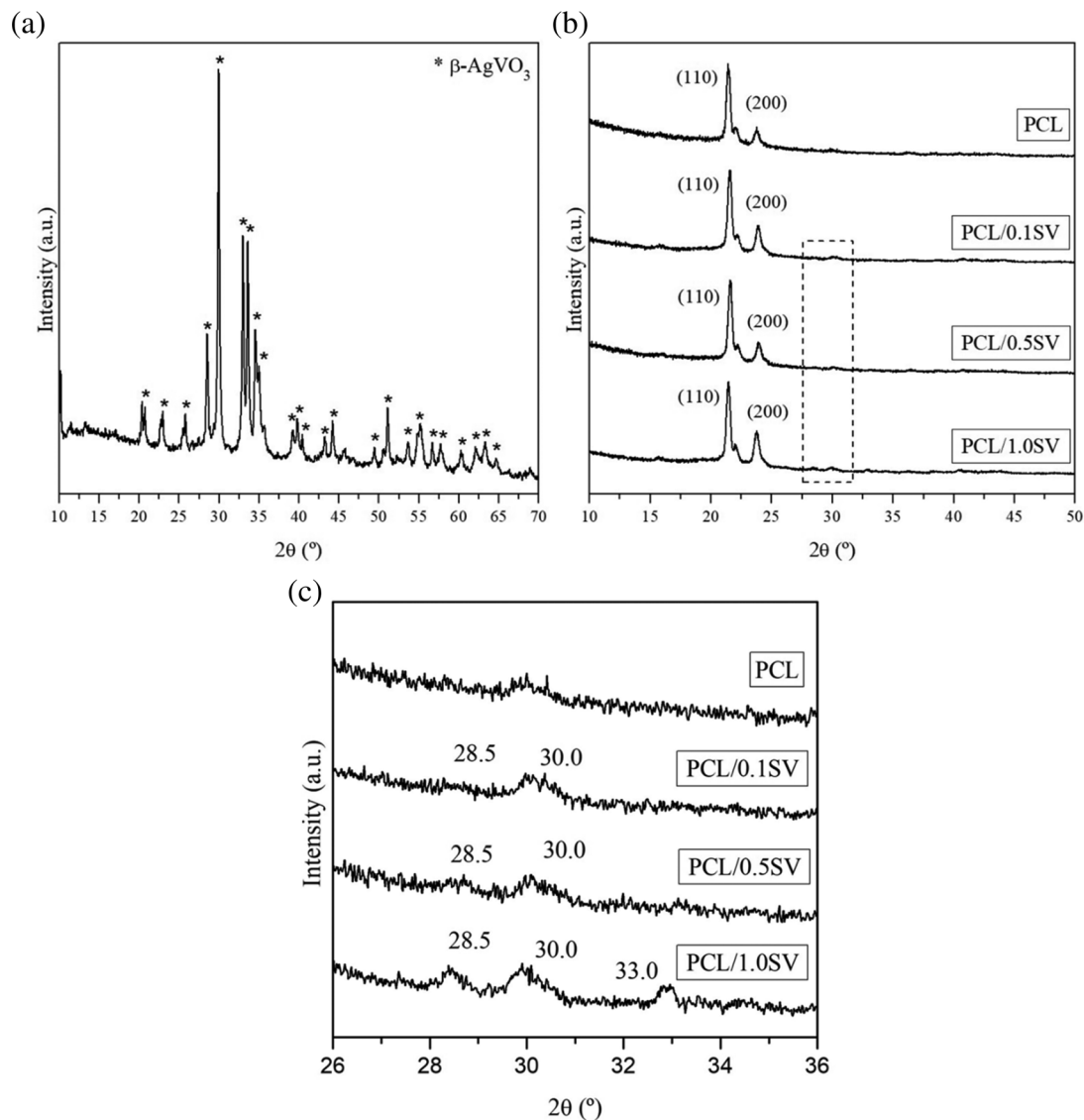


**FIGURE 2** (a) X-ray diffraction (XRD) patterns of SV, (b) XRD patterns of PCL, PCL/0.1SV, PCL/0.5SV, and PCL/1.0SV, and (c) focused peaks between 26 and 36° for PCL, PCL/0.1SV, PCL/0.5SV, and PCL/1.0SV

**TABLE 3** Crystallinity degree, crystallite size, and lattice parameters of neat PCL and nanocomposites

Sample	$2\theta$ (°)	C (nm)	$X_c$ (%)	Lattice parameters		
				a (Å)	b (Å)	c (Å)
PCL	21.4	21.1	88.5	6.7	5.3	16.1
PCL/0.1SV	21.6	19.0	83.6	6.6	5.3	17.0
PCL/0.5SV	21.6	20.0	80.5	6.6	5.3	17.0
PCL/1.0SV	21.4	20.3	76.4	6.7	5.3	17.5

which lead to a faster crystallization rate. In this way, SV nanorods probably reduce the mobility of PCL molecular chains during the crystallization process, hampering the complete crystallization.<sup>69</sup> According to Table 3, higher incorporation of SV nanorods resulted in lower  $X_c$

values. The incorporation of large number of nanoparticles in a polymeric matrix will lead to an increased formation of nucleating sites. As result, a faster crystallization will happen, producing a less perfect arrangement.

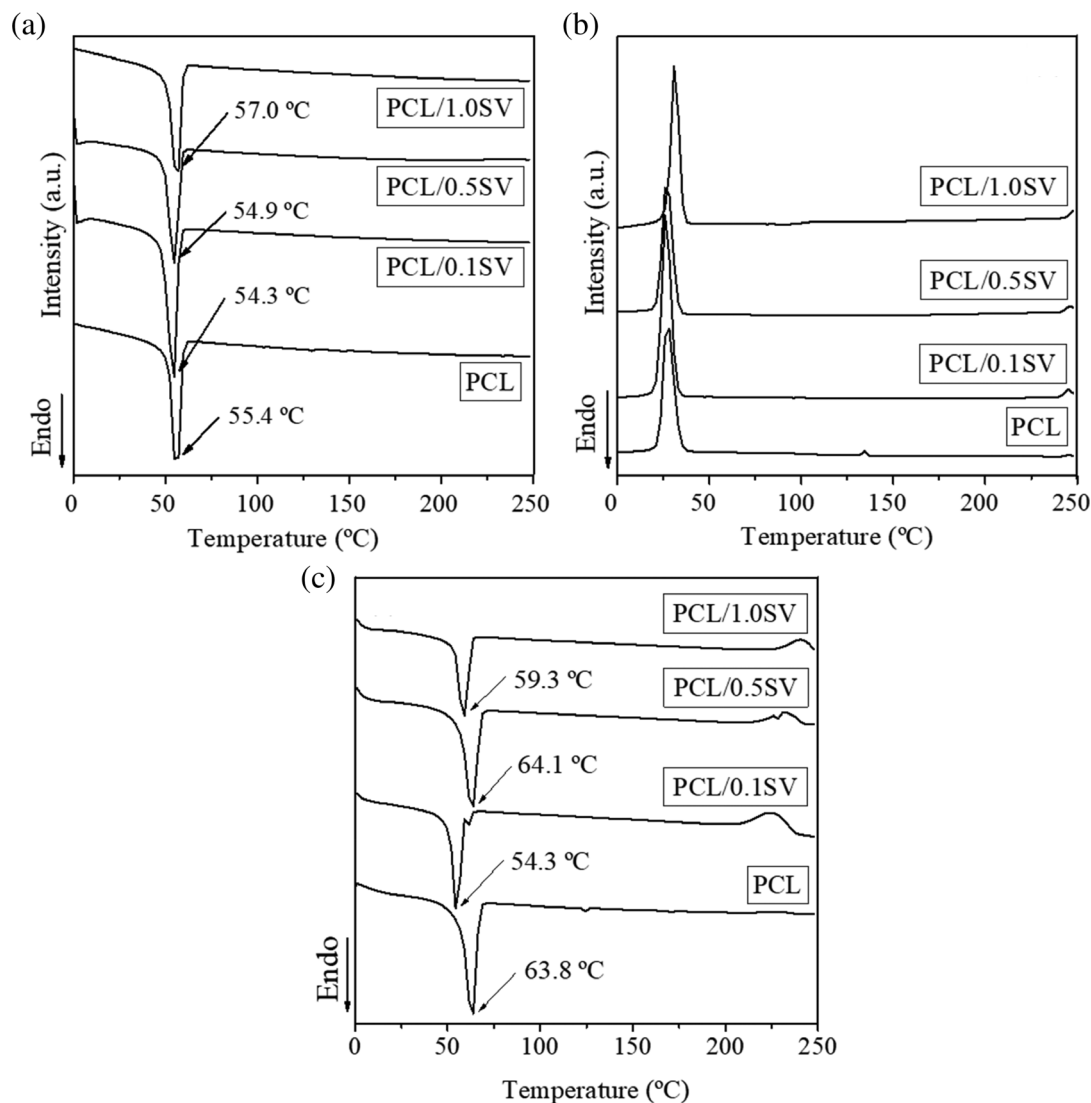


**FIGURE 3** Differential scanning calorimetry thermograms of (a) first heating, (b) cooling, and (c) second heating for neat PCL, PCL/0.1SV, PCL/0.5SV, and PCL/1.0SV

From the XRD results, it can be concluded that SV has a substantial effect on PCL crystallization, reducing the crystallinity degree.<sup>72</sup> These values are in accordance with the results obtained by Raman spectroscopy, which showed the widening of the band at  $1720\text{ cm}^{-1}$ , associated with the growth of amorphous domains. On the other hand, properties as crystallite size and lattice parameters were not affected, maintaining the primary structure of the polymer. These results indicate that the incorporation of SV nanorods into PCL led to a limit disordered effect, since it interfered only in the arrangement of polymeric chains in the long range.<sup>71</sup>

### 3.4 | Differential scanning calorimetry

Figure 3 presents the DSC curves of first heating, cooling, and second heating of neat PCL and its nanocomposites;

and Table 4 shows the thermal characteristics derived from the DSC curves, which have the purpose of presenting and identifying the transition temperatures.

In the first heating (Figure 3(a)), an endothermic peak of melting temperature ( $T_m$ ), at 55.4, 54.3, 54.9, and 57.0°C was observed for neat PCL, PCL/0.1SV, PCL/0.5SV, and PCL/1.0SV, respectively. The melting temperature of neat PCL in this study is in agreement with the literature.<sup>10</sup> The  $T_m$  of PCL/0.1 SV and PCL/0.5 SV nanocomposites was unaltered, when compared with neat PCL. However, the  $T_m$  of PCL/1.0SV, sample with highest concentration of SV, was slightly shifted to a higher temperature (2.8% increase).

Furthermore, significant changes were observed in the melting temperature in the second heating (Figure 3(c)), more specifically in the samples of neat PCL, PCL/0.5SV, and PCL/1.0SV, in which the  $T_m$  values were increased. In general, for semi crystalline



**TABLE 4** DSC analysis, Melting temperature ( $T_m$ ) and degree of crystallinity ( $X_c$ ), from first and second heating, crystallization temperature ( $T_c$ ) from cooling

Samples	First heating		Cooling $T_c$ (°C)	Second heating	
	$T_m$ (°C)	$X_c$ (%)		$T_m$ (°C)	$X_c$ (%)
PCL	55.4	50.4	26.6	63.8	73.5
PCL/0.1 SV	54.9	51.4	26.5	54.3	68.1
PCL/0.5 SV	54.9	50.2	27.0	64.1	66.6
PCL/1.0 SV	57.0	41.7	29.4	59.3	48.1

polymers, the molecular chains can be partly in the crystal and partly in the surrounding melt during the process of heating. In this way, with increasing temperature, a small fraction of the chain can be removed from the crystal and transferred to the melt phase. Also with a decrease in the temperature, the molecular chain can be attached again to the crystal. This event does not happen likewise to the initial stage, meaning that the attachment may happen in a different position. Moreover, it may have a larger part inside or around the crystal, what could be influenced by the rate of heating and/or cooling. In those mechanisms, known as “reversible process”, segments of the same macromolecule can be attached or detached from the crystal without the need of nucleation sites, only with variation in temperature. When the polymer is heated again, the behavior may be different from the first heating, and as a result, a difference in the melting or crystallization temperature is observed.<sup>11,73</sup> In this case, this differences in the melting temperature comparing the first and second heating can be justified by the reversible process.

Concerning the exothermic peak from the cooling process (Figure 3(b) and Table 4), the crystallization temperature ( $T_c$ ) showed no significant changes between the neat PCL and the nanocomposites PCL/0.1SV and PCL/0.5SV. However, there was an increase of approximately 10.5% in  $T_c$  values for PCL/1.0 SV, compared with neat PCL. According to the literature, a higher  $T_c$  demonstrates that the polymer have an increased number of nucleation sites during crystallization.<sup>74,75</sup> Thus, a greater crystallization capacity will be achieved when the amount of energy for crystallization is low. When adding SV nanoparticles to the PCL matrix, the crystallization temperature slightly increased, especially for the nanocomposite with 1.0% of SV nanoparticles in the PCL matrix. This is an indication that SV nanoparticles may have acted as a heterogeneous nucleating agent, besides having influenced in the nucleation free energy for the PCL matrix.<sup>76</sup> Kong et al<sup>77</sup> reported the same behavior by adding a bioresource starch-based nanoparticles (SNPs) in the PCL matrix.

Another study, in which the same behavior was observed, was carried out by Jiao et al,<sup>78</sup> which developed composites based on hydroxyapatite (HA) (20 wt%) and polycaprolactone (PCL) by melt blending process, for application in tissue engineering scaffolds. In this study, the authors verified that the addition of the HA particles made the PCL molecular chain absorbed on the surface of HA and contributed to heterogeneous nucleation, increasing the crystallization rate of PCL, and crystallization ability.

According to Table 4, both values of  $X_c$ , in the first as well as in the second heating, showed a reduction as the content of SV nanoparticles increased in the PCL matrix. However, in the first heating, PCL/0.1SV and PCL/0.5SV samples did not show differences in  $X_c$  values when compared with neat PCL, only the sample with the highest content of SV nanoparticles (PCL/1.0SV), showed a significant reduction of 17.2% in  $X_c$  values.

Concerning the  $X_c$  values from the second heating, all nanocomposites showed a significant reduction, being 7.3%, 9.4%, and 34.5%, for PCL/0.1SV, PCL/0.5SV, and PCL/1.0SV, respectively, compared with neat PCL. Thus, the presence of SV nanoparticles in the PCL matrix influenced the crystallization behavior, decreasing the  $X_c$  of the nanocomposites. The crystallinity degree measured by XRD showed similar behavior. A reduction in the crystallinity degree was also observed, being 5.5%, 9.0%, and 13.6% for PCL/0.1SV, PCL/0.5SV, and PCL/1.0SV, respectively, compared with neat PCL. Some minor difference between the  $X_c$  values obtained by XRD (Table 3) and DSC (Table 4) was observed. These small differences might be caused by the different nature of analysis, since DSC measures crystallinity during the heating process while XRD measures the polymer structure at an equilibrium state with solid morphologies.<sup>79</sup> However, even with these discrepancies among the  $X_c$  results, both DSC and XRD showed a pattern in crystallinity results: smaller crystallinity for the nanocomposites with higher number of nanorods.

Usually, the crystallization process is composed of two main mechanisms: nucleation and growth. The

addition of SV nanoparticles resulted in a high nucleation and a faster crystallization rate, producing a less perfect arrangement and smaller stacking of molecular chains.<sup>74–76</sup> Furthermore, higher content of nanoparticles in the PCL matrix, influenced the lower the  $X_c$  value. Therefore, the reduction in the  $X_c$  values for the nanocomposites compared to the neat PCL, may be related to the growth of the crystals during the crystallization. Due to space restrictions and the high nucleation rate, combined with the low mobility of the molecular chains, a great number of nuclei collide and limit their growth, hindering complete crystallization, and consequently, decreasing the  $X_c$  values of the nanocomposites. These values are in accordance with the results reported by XRD and Raman. This same behavior was reported by Li et al.<sup>80</sup>

Furthermore, this reduction in the  $X_c$  values of the PCL/SV nanocomposites, may be related to the size of the vanadate nanoparticles, because in addition to the good dispersion, the nanoparticles had large sizes,<sup>22</sup> which may have made crystallization difficult. Similar behavior was observed by Montanheiro et al.,<sup>81</sup> which studied the influence of the pre-dispersion of carbon nanotube (CNT) in the poly(3-hydroxybutyrate-co-3-hydroxyvalerate) (PHBV) matrix to obtain nanocomposites PHBV/CNT.

### 3.5 | Transmission and scanning electron microscopy

Figure 4 shows SV morphological characteristic obtained by FEG-SEM and TEM analyses. FEG-SEM images (Figure 4(a)) shows the nanorod structure with diameters of about 60 nm and length of several micrometers, and smooth surfaces. The rod-like SV morphology was confirmed by high-resolution TEM images (Figure 4(b)), which reveals a strong contrast between the SV nanorods

and homogeneous circular nanoparticles on SV surfaces, with diameters of about 15 nm.<sup>82</sup> Those circular nanoparticles are AgNPs anchored on the SV nanorod surfaces. AgNPs precipitates on SV surfaces through  $\text{AgNO}_3$  reduction ( $\text{Ag}^+$  to  $\text{Ag}^0$ ).<sup>83</sup> The large atomic number difference between SV nanorods and AgNPs results in a strong contrast, being the AgNPs darker in TEM image. The AgNPs decorated on SV nanorods are expected to exhibit enhanced antimicrobial performance, since the antimicrobial activity happens with the contact between the bacteria and  $\text{Ag}^+$  ions released by Ag-decorated SV.<sup>29</sup>

Figure 5 shows the morphological surface of neat PCL, PCL/0.1SV, PCL/0.5SV, and PCL/1.0SV nanocomposite films. All samples present smooth surface, with small pores, resulting from the solvent evaporation process. The same morphological surface with the presence of pores was observed by Natu, Sousa, and Gil<sup>84</sup> and Siqueira et al.<sup>85</sup> According to Li et al.,<sup>86</sup> the final morphology of PCL is also strongly influenced by the volatility of solvents. Thus, when the evaporating ability of the solvent is high, time is not enough for PCL molecular chains to align along, in the presence or not of particles, loads, and others, for example. Furthermore, this final PCL morphology is called epitaxial crystals.

Figure 6 shows the morphological cryo-fractured surfaces of neat PCL, PCL/0.1SV, PCL/0.5SV, and PCL/1.0SV nanocomposites. The cryogenic fracture was performed in order to verify the homogeneity and dispersion of SV nanoparticles into the PCL matrix; and the neat PCL sample was used as a comparison standard.

In Figure 6(a) the cryo-fractured surface of PCL is smooth and homogeneous, when compared with the PCL/SV nanocomposites (Figures 6(b)-(d)). Regarding the nanocomposites, all samples have rougher morphological surfaces compared with neat PCL, but with good

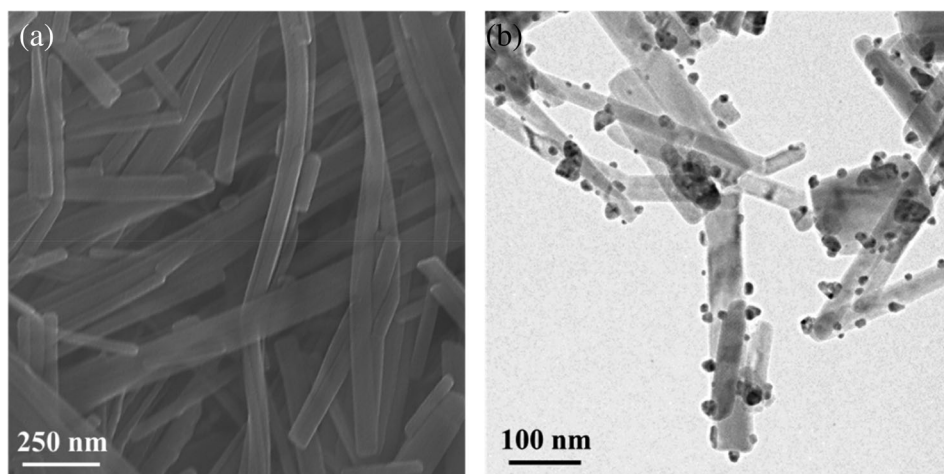


**FIGURE 4** SV images obtained by (a) FEG-SEM, and (b) TEM

**FIGURE 5** SEM micrographs of (a) neat PLC, (b) PCL/0.1SV, (c) PCL/0.5 SV, and (d) PCL/1.0 SV, with 500× magnification

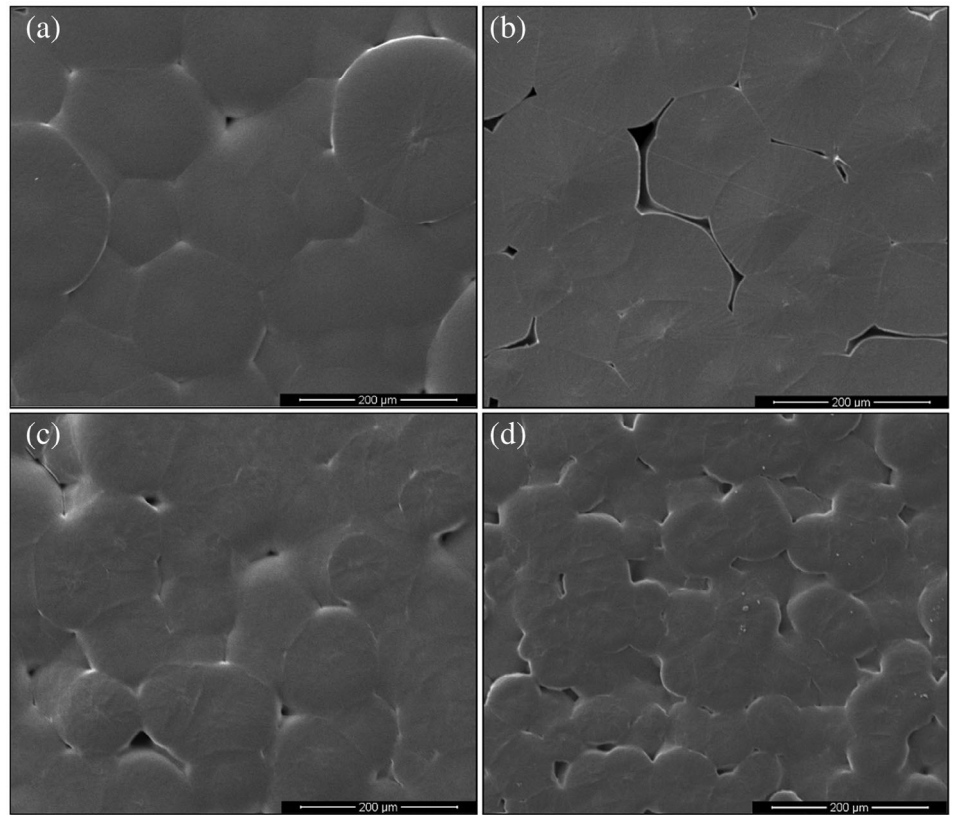
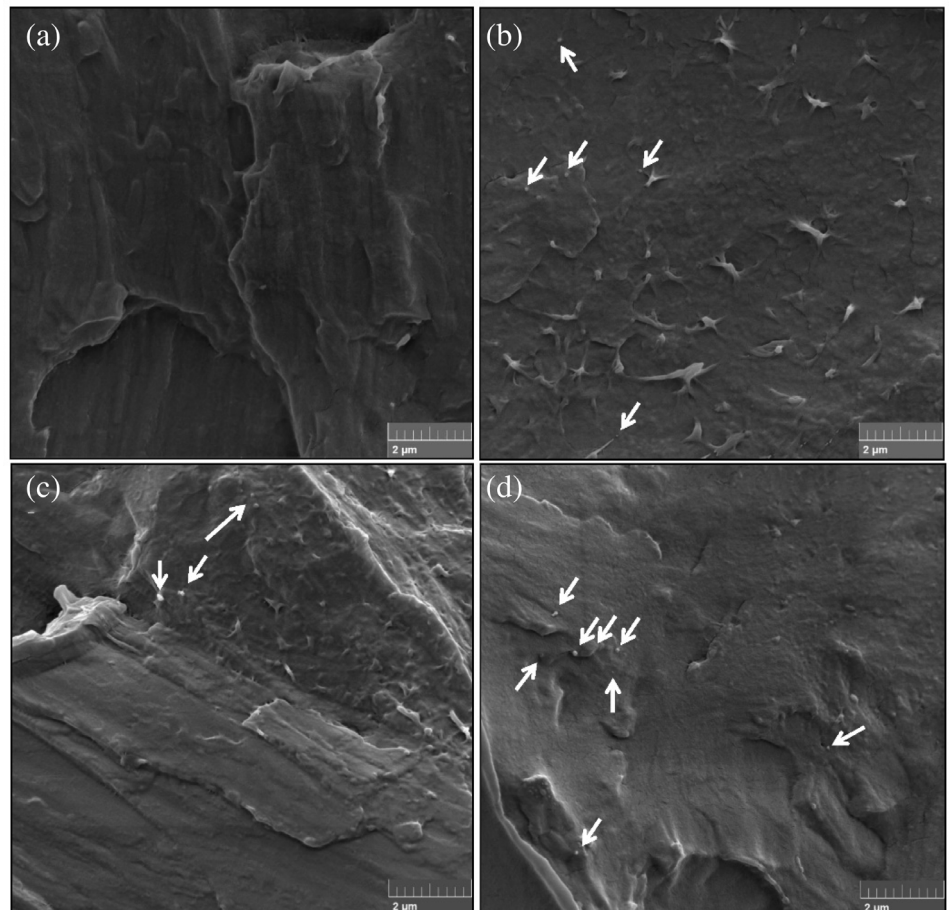


**FIGURE 6** FEG-SEM micrographs of the cryo-fracture surface: (a) neat PCL, (b) PCL/0.1SV, (c) PCL/0.5SV, and (d) PCL/1.0V





distribution of the SV nanoparticles in the PCL matrix (identified with white arrows in the micrographs).

Hydrophilic particles, when dispersed in a hydrophobic and nonpolar matrix, as the case of SV nanoparticles and the PCL matrix, respectively, could result in low adhesion between particle/matrix and poor dispersion. Thus, the good dispersion and adhesion of the SV nanoparticles in the PCL matrix, which was observed in the present work, may be due to the methodology used to obtain the nanocomposites, which proved to be viable and efficient. Li et al.<sup>80</sup> analyzed the cryofractured surface of PCL and nanocellulose (NC) nanocomposites, and reported morphology very similar to that observed in the present work.

### 3.6 | Antimicrobial activity

The antimicrobial activity of the films against *Staphylococcus aureus* and *Escherichia coli* was tested to evaluate the application of PCL/SV films as biomaterials. Sterility tests did not detect contamination of the specimens, proving the efficacy of the adopted sterilization method. No inhibition halos were observed for both *S. aureus* and *E. coli* in the agar diffusion method.

Figure 7(a) shows the results obtained for antibacterial activity of neat PCL and nanocomposites with SV and the control group on *S. aureus* using the direct contact test.

Significative reduction in *S. aureus* viable cell counts was observed for the groups with neat PCL ( $p = 0.05$ ) and PCL/1.0SV ( $p = 0.03$ ), when compared with control group. The bacterial reduction for PCL/1.0SV was 52% when compared with the control and 7% when compared with neat PCL. No significant reduction in the counts of *S. aureus* was observed for the groups with PCL/0.1SV

and PCL/0.5SV when compared the control group. However, reductions of 24% and 33% were observed for PCL/0.1SV and PCL/0.5SV, respectively, when compared with the control.

For *E. coli*, no significant reduction in viable cells count in relation to the control was observed, although the PCL/1.0SV group showed a reduction in the average concentration of *E. coli* (Figure 7(b)). For this sample, a reduction of 42% was observed when compared to the control, and of 5% when compared with neat PCL. Samples PCL/0.1SV and PCL/0.5SV showed a bacterial reduction of 32% and 29%, respectively, compared to the control. The differences of response between Gram-positive and Gram-negative bacteria can be related to the morphological differences in their cell wall and in the thickness of peptidoglycan layer that can result in differences in susceptibility to antimicrobial compounds.<sup>87–89</sup>

Antibacterial activity of PCL/1.0SV in liquid medium on *S. aureus* was observed in this study. Samples with lower concentrations did not show statistically significant antibacterial activity, which may be explained by the small concentration of SV present in the sample, and possibility of embedment of the filler by the polymer. This behavior is commonly observed in polymer composites with good interaction between the filler and the matrix.<sup>81,90,91</sup>

Higher filler concentrations would probably result in some amount of exposed SV on the samples surface, allowing the antimicrobial effect of SV. These data corroborate that found by Castro et al.<sup>92</sup> who tested acrylic resin incorporated with SV particles in different concentrations, using the agar diffusion method. The authors observed antibacterial action from the concentration of 2.5% SV in *S. aureus*. Kreve et al, (2019)<sup>29</sup> noticed in the same methodology that SV particles mixed in denture

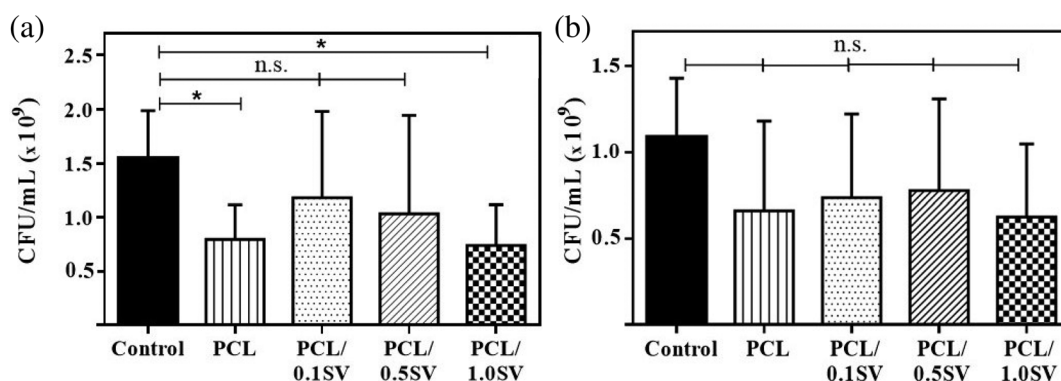


**FIGURE 7** Concentration of (a) *Staphylococcus aureus* and *Escherichia coli* (b) (colony forming units per milliliter, CFU ml<sup>-1</sup>) after 24 h of contact with neat PCL and PCL/SV nanocomposites. The results are represented by the mean and standard deviation. ANOVA was applied followed by Dunnett's multiple comparison test. \*, Significant difference. N.S., non-significant difference

resin, in concentrations of 1%, 2.5%, 5%, and 10% did not show antibacterial action on *S. aureus*.

The differences in the results of antimicrobial activity obtained by agar diffusion and direct contact methodologies, suggest that higher concentrations of  $\text{Ag}^+$  ions are not capable of leaving PCL's surface and diffuse through the agar. In fact, some works have showed that  $\beta\text{-AgVO}_3$  nanorods presents the leaching of  $\text{Ag}^+$  ions by less than 1%. In this way,  $\beta\text{-AgVO}_3$  antibacterial activity is mostly due to the contact between the PCL/SV films and the bacteria.<sup>93</sup> The porous morphology of the films (Figure 4) favors the antibacterial effect in liquid medium and the absence of effect in solid medium. The liquid medium has better contact with the surface, penetrating into the pores and increasing the possibility to have contact with some exposed SV nanorods and Ag ions.

On the other hand, in the agar diffusion method, the need of diffusion of the substance through the agar is considered one limitation. As observed in Figure 4, no exposed SV is observed on the film's surfaces. In this way, there is no contact between the solid agar and the SV particles, responsible for the antimicrobial activity. This fact may be responsible for the absence of antimicrobial activity in solid agar.

The antibacterial effect of  $\text{AgVO}_3$  stems from the the contact of  $\text{Ag}^+$  ions with different bacterial cellular targets, causing loss of cellular function.<sup>20</sup> DNA, proteins, and cellular membrane are the most affected targets, inhibiting replication and causing morphological changes and oxidative stresses due to reactive oxygen species.<sup>94</sup>  $\text{Ag}^+$  ions interacts with thiol groups in proteins, inducing to the inactivation of bacterial proteins. Also, these ions alter DNA molecules, hindering bacterial replication.<sup>94</sup>

This finding can expand the applications of the PCL polymer incorporated with SV as biomedical material for production of scaffolds, catheters, and membranes with combined antimicrobial activity and cell proliferation. Those biomaterials are usually used in contact with liquid medium of the human body, favoring the  $\text{Ag}^+$  ions release and avoiding infections by pathogenic microorganisms. Further studies are necessary to improve the antibacterial activity of the PCL/SV nanocomposites without compromising their biocompatibility. Higher amounts of SV added to the PCL matrix will probably enhance the antibacterial activity; however, the cytotoxicity can also be increased.

## 4 | CONCLUSIONS

This article reported the production and characterization of PCL/SV nanocomposites, by a simple methodology, and with potential results to be applied as biomaterial with

antimicrobial activity. FTIR spectroscopy showed good interaction between the PCL matrix and the SV particles, which was confirmed by SEM. TEM images showed a rod-like morphology for SV with AgNPs decorating its surfaces. The addition of SV into the PCL matrix caused a reduction in the size of crystallites and in the overall crystallinity, which could be advantageous for some mechanical properties. The sample produced with 1 wt% of SV into PCL exhibited antibacterial activity against *S. aureus* in direct contact test, expanding the range of possible applications of this material. The antibacterial activity is mostly resultant of  $\text{Ag}^+$  ions released by AgNPs on SV nanorods surfaces. Higher concentrations of SV incorporated into the PCL matrix could result in even better antimicrobial activity and efficiency against other microbial species.


## ACKNOWLEDGMENTS

The authors gratefully acknowledge the Associated Laboratory of Sensors and Materials in the National Institute for Space Research (LABAS/INPE) for FEG-SEM images. This study was funded by the Brazilian Funding institutions FAPESP (Fundação de Amparo à Pesquisa do Estado de São Paulo) [2017/24873-4; 2018/12035-7, 2017/02846-5], FINEP (Financiadora de Estudos e Projetos) [01.13.0328.03] and CAPES (Coordenação de Aperfeiçoamento de Pessoal de Nível Superior).

## CONFLICT OF INTEREST

The authors declare no potential conflict of interest.

## ORCID

Beatriz Rossi Canuto de Menezes  <https://orcid.org/0000-0001-9605-3921>

Thais Larissa do Amaral Montanheiro  <https://orcid.org/0000-0003-4230-8161>

Aline da Graça Sampaio  <https://orcid.org/0000-0001-9453-3905>

Cristiane Yumi Koga-Ito  <https://orcid.org/0000-0002-2416-2173>

Gilmar Patrocínio Thim  <https://orcid.org/0000-0001-6410-3031>

Larissa Stieven Montagna  <https://orcid.org/0000-0002-7947-3112>

## REFERENCES

- [1] R. Greenhalgh, N. C. Dempsey-hibbert, K. A. Whitehead, *Int. Biodeterior. Biodegradation* **2019**, 136, 1.
- [2] R. L. M. S. Oliveira, L. Barbosa, C. R. Hurtado, et al., *J. Biomed. Mater. Res. Part A* **2020**, 1.
- [3] J. L. Castro-Mayorga, M. J. Fabra, J. M. Lagaron, *Innov. Food Sci. Emerg. Technol.* **2016**, 33, 524.
- [4] A. Tiwari, *Handbook of Antimicrobial Coatings*, 1st ed., Elsevier Inc., Amsterdam **2017**, p. 27.



- [5] M. S. Hasnain, S. A. Ahmad, N. Chaudhary, et al., *Applications of Nanocomposite Materials in Orthopedics*, 1st ed., Elsevier Inc., Amsterdam **2019**, p. 1.
- [6] F. J. Van Natta, J. W. Hill, W. H. Carothers, *J. Am. Chem. Soc.* **1934**, 1772, 5.
- [7] T. K. Dash, V. B. Konkimalla, *J. Control Release.* **2012**, 158, 15.
- [8] D. Chen, J. Bei, S. Wang, *Polym. Degrad. Stab.* **2000**, 67, 455.
- [9] R. M. Mohamed, K. Yusoh, *Adv. Mater. Res.* **2015**, 1134, 249.
- [10] M. Labet, W. Thielemans, *Chem. Soc. Rev.* **2009**, 38, 3484.
- [11] B. Wunderlich, *Prog. Polym. Sci.* **2003**, 28, 383.
- [12] A. Hudecki, G. Kiryczyn, M. J. Los, *Stem Cells and Biomaterials for Regenerative Medicine*, 1st ed., Elsevier Inc., Amsterdam **2019**, p. 85.
- [13] D. Mondal, M. Griffith, S. S. Venkatraman, *Int. J. Polym. Mater. Polym. Biomater.* **2016**, 4037, 255.
- [14] H. S. Yu, J. Park, H. Lee, et al., *World J. Mens Heal.* **2018**, 36, 66.
- [15] A. Manakhov, E. S. Permyakova, S. Ershov, A. Sheveyko, A. Kovalskii, J. Polčák, I. Y. Zhitnyak, N. A. Gloushankova, L. Zajíčková, D. V. Shtansky, *Appl. Surf. Sci.* **2019**, 479, 796.
- [16] M. Assunta, G. Gomez, M. Malinconico, et al., *Mater. Sci. Eng. C.* **2015**, 48, 457.
- [17] H. Zhu, J. Shen, X. Feng, H. Zhang, Y. Guo, J. Chen, *Mater. Sci. Eng. C.* **2010**, 30, 132.
- [18] H. Li, Chang, *Biomaterials* **2004**, 25, 5473.
- [19] S. S. D. Kumar, N. K. Rajendran, N. N. Houreld, H. Abrahamse, *Int. J. Biol. Macromol.* **2018**, 115, 165.
- [20] D. T. De Castro, M. L. C. Valente, C. H. L. Da Silva, et al., *Arch Oral Biol.* **2016**, 67, 46.
- [21] R. D. Holtz, A. G. Souza Filho, M. Brocchi, D. Martins, N. Durán, O. L. Alves, *Nanotechnology* **2010**, 21, 185102.
- [22] B. R. C. de Menezes, R. Guimarães, V. M. Schatkoski, et al., *SN Appl. Sci.* **2019**, 1, 1327.
- [23] M. Pudukudy, Q. Jia, H. Wang, S. Shan, R. Rajendran, *Mater. Sci. Semicond Process.* **2020**, 107, 104824.
- [24] B. N. A. S. Pimentel, C. C. Foggi, et al., *Mater. Sci. Eng. C.* **2019**, 108, 110405.
- [25] S. Kittaka, K. Matsuno, H. Akashi, *J. Solid State Chem.* **1999**, 367, 360.
- [26] J. L. Falcone, D. W. Grainger, *Comprehensive Biomaterials II*, 2nd ed., Elsevier Inc., Amsterdam **2017**, p. 79.
- [27] T. Chen, M. Shao, H. Xu, C. Wen, S. T. Lee, *J. Colloid Interface Sci.* **2012**, 366, 80.
- [28] T. A. Vu, C. D. Dao, T. T. T. Hoang, P. T. Dang, H. T. K. Tran, K. T. Nguyen, G. H. le, T. V. Nguyen, G. D. Lee, *Mater. Lett.* **2014**, 123, 176.
- [29] S. Kreve, V. C. Oliveira, L. Bachmann, O. L. Alves, A. C. D. Reis, *Sci. Rep.* **2019**, 9, 11889.
- [30] A. P. de Melo Monteiro, R. Dias Holtz, L. Carneiro Fonseca, et al., *Chem. Rec.* **2018**, 18, 973.
- [31] S. Y. C. Tong, J. S. Davis, E. Eichenberger, T. L. Holland, V. G. Fowler Jr., *Clin. Microbiol. Rev.* **2015**, 28, 603.
- [32] F. Alam, K. Balani, *J. Mech. Behav Biomed. Mater.* **2017**, 65, 872.
- [33] L. E. Fisher, A. L. Hook, W. Ashraf, A. Yousef, D. A. Barrett, D. J. Scurr, X. Chen, E. F. Smith, M. Fay, C. D. J. Parmenter, R. Parkinson, R. Bayston, *J. Control Release.* **2015**, 202, 57.
- [34] A. G. Karakeçili, M. Gümüşderehoğlu, *J. Biomater. Sci. Polym. Ed.* **2002**, 13, 185.
- [35] C. Lüdecke, K. D. Jandt, D. Siegismund, M. J. Kujau, E. Zang, M. Rettenmayr, J. Bossert, M. Roth, *PLoS One* **2014**, 9, e84837.
- [36] M. A. Fanovich, J. Ivanovic, D. Misic, et al., *J. Supercrit. Fluids.* **2013**, 78, 42.
- [37] R. Augustine, H. N. Malik, D. K. Singhal, A. Mukherjee, D. Malakar, N. Kalarikkal, S. Thomas, *J. Polym. Res.* **2014**, 21, 347.
- [38] M. S. Brzezinska, M. Walczak, U. Jankiewicz, M. Pejchalová, *J. Polym. Environ.* **2018**, 26, 589.
- [39] Z. Li, N. Wu, J. Cheng, M. Sun, P. Yang, F. Zhao, J. Zhang, X. Duan, X. Fu, J. Zhang, X. Hu, H. Chen, Y. Ao, *Theranostics* **2020**, 10, 5090.
- [40] L. S. Montagna, T. L. D. A. Montanheiro, F. R. Passador, et al., *J. Polym. Environ.* **2017**, 26, 1511.
- [41] T. L. A. Montanheiro, F. H. Cristóvan, A. P. Lemes, *J. Mater. Res.* **2015**, 30, 55.
- [42] T. L. A. Montanheiro, L. S. Montagna, J. P. B. Machado, et al., *Polym. Compos.* **2019**, 40, 288.
- [43] J. Cai, Z. Xiong, M. Zhou, J. Tan, F. Zeng, MeihuMa, S. Lin, H. Xiong, *Carbohydr. Polym.* **2014**, 102, 746.
- [44] V. Crescenzi, G. Manzini, G. Calzolari, C. Borri, *Eur. Polym. J.* **1972**, 8, 449.
- [45] CLSI, *Methods for Dilution Susceptibility Test for Bacteria That Grow Aerobically, Approved Standard (M07-A10)*, 7th ed. Clinical and Laboratory Standards Institute, Wayne **2006**.
- [46] L. A. D. Koslowski, A. L. Nogueira, S. Licodiedoff, et al., *Rev Ambient Água.* **2018**, 13(6), e1947.
- [47] V. Trakoolwannachai, P. Kheolamai, S. Ummartyotin, *Compos. Part B Eng.* **2019**, 173, 106974.
- [48] F. Sharif, S. Tabassum, W. Mustafa, A. Asif, F. Zarif, M. Tariq, S. A. Siddiqui, M. A. Gilani, I. Ur Rehman, S. MacNeil, *Polym. Compos.* **2019**, 40, 1564.
- [49] T. F. da Silva, G. F. d. M. Morgado, T. L. d. A. Montanheiro, et al., *SN Appl. Sci.* **2020**, 2, 369.
- [50] H.-Y. Mi, X. Jing, J. Peng, M. R. Salick, X. F. Peng, L. S. Turng, *Cellulose* **2014**, 21, 2727.
- [51] A. K. Gaharwar, P. J. Schexnailder, G. Schmidt, *Nanobiomaterials Handbook*, CRC Press, New York **2011**, 24–1.
- [52] N. Roy, R. Sengupta, A. K. Bhowmick, *Prog. Polym. Sci.* **2012**, 37, 781.
- [53] M. T. Byrne, W. P. McNamee, Y. K. Gun'ko, *Nanotechnology* **2008**, 19, 415707.
- [54] D. R. Paul, L. M. Robeson, *Polymer* **2008**, 49, 3187.
- [55] B. R. C. Menezes, M. T. Campos, L. T. Montanheiro, et al., *J. Compos. Sci.* **2019**, 3, 21.
- [56] L. S. Montagna, T. L. d. A. Montanheiro, M. JPB, et al., *Int. J. Polym. Sci.* **2017**, 2017, 9316761.
- [57] M. Silva, N. M. Alves, M. C. Paiva, *Polym. Adv. Technol.* **2018**, 29, 687.
- [58] C. Geng, X. Hu, G. Yang, Q. Zhang, F. Chen, Q. Fu, *Chinese J. Polym. Sci.* **2015**, 33, 61.
- [59] H. X. Xiang, S. H. Chen, Y. H. Cheng, et al., *Express Polym. Lett.* **2013**, 9, 778.
- [60] F. V. Ferreira, A. Dufresne, I. F. Pinheiro, D. H. S. Souza, R. F. Gouveia, L. H. I. Mei, L. M. F. Lona, *Eur. Polym. J.* **2018**, 108, 274.
- [61] A. Giri, T. Bhunia, A. Pal, L. Goswami, A. Bandyopadhyay, *Eur. Polym. J.* **2016**, 74, 13.
- [62] J.-M. Song, Y.-Z. Lin, H.-B. Yao, F. J. Fan, X. G. Li, S. H. Yu, *ACS Nano.* **2009**, 3, 653.

- [63] V. Sessini, I. Navarro-Baena, M. P. Arrieta, F. Dominici, D. López, L. Torre, J. M. Kenny, P. Dubois, J. M. Raquez, L. Peponi, *Polym. Degrad. Stab.* **2018**, *152*, 126.
- [64] A. Kołodziej, A. Weselucha-Birczyńska, M. Świętek, Ł. Skalniak, M. Błażewicz, *Int. J. Polym. Mater. Polym. Biomater.* **2019**, *68*, 44.
- [65] S. Vijayavenkataraman, S. Thaharah, S. Zhang, W. F. Lu, J. Y. H. Fuh, *Artif. Organs.* **2019**, *43*, 515.
- [66] H. Bittiger, R. H. Marchessault, W. D. Niegisch, *Acta Crystallogr. Section B.* **1970**, *26*, 1923.
- [67] Y. Chatani, Y. Okita, H. Tadokoro, Y. Yamashita, *Polym. J.* **1970**, *1*, 555.
- [68] A. S. K. Kiran, T. S. S. Kumar, R. Sanghavi, et al., *Nanomaterial* **2018**, *8*, 860.
- [69] M. Xie, B. Wang, P. Zhang, *J. Dispers. Sci. Technol.* **2019**, *40*, 94.
- [70] F. Benhacine, A. Ouargli, A. S. Hadj-Hamou, *Polym. Technol. Mater.* **2019**, *58*, 328.
- [71] E. Piorkowska, G. C. Rutledge, *Handbook of Polymer Crystallization*, 1st ed., John Wiley and Sons, New Jersey **2013**, p. 31.
- [72] Y. Suzuki, H. Duran, W. Akram, M. Steinhart, G. Floudas, H. J. Butt, *Soft Matter.* **2013**, *9*, 9189.
- [73] I. Okazaki, B. Wunderlich, *Macromolecules* **1997**, *9297*, 1758.
- [74] H. Yokota, T. Kawakatsu, *Polymer* **2020**, *186*, 121975.
- [75] D. Turnbull, *J. Chem. Phys.* **1950**, *98*, 198.
- [76] A. M. Rhoades, M. Laura, D. Lorenzo, et al., *Handbook of Thermal Analysis and Calorimetry*, 1st. ed., Vol. 7, Elsevier Inc., Amsterdam **2018**, p. 253.
- [77] J. Kong, Y. Yu, X. Pei, C. Han, Y. Tan, L. Dong, *Int. J. Biol. Macromol.* **2017**, *102*, 1304.
- [78] Z. Jiao, B. Luo, S. Xiang, H. Ma, W. Y. Yuan Yu, *Adv. Ind. Eng. Polym. Res.* **2019**, *2*, 196.
- [79] R. Salehiyan, S. S. Ray, V. Ojijo, *Macromol. Mater. Eng.* **2018**, *303*, 1800349.
- [80] Y. Li, C. Han, Y. Yu, L. Xiao, *Int. J. Biol. Macromol.* **2020**, *147*, 34.
- [81] T. L. Montanheiro, C. TMB, M. LSS, et al., *Mater. Res. Express* **2019**, *6*, 105375.
- [82] S. Liang, J. Zhou, X. Zhang, Y. Tang, G. Fang, T. Chen, X. Tan, *CrystEngComm.* **2013**, *15*, 9869.
- [83] D. McNulty, Q. Ramasse, C. O'Dwyer, *Nanoscale* **2016**, *8*, 16266.
- [84] V. Natu, S. H. C. De, M. H. Gil, *Polym. Degrad. Stab.* **2013**, *98*, 44.
- [85] I. A. W. B. Siqueira, N. Koba, D. Moura, et al., *Mater. Lett.* **2017**, *206*, 210.
- [86] S. Li, X. Sun, H. Li, S. Yan, *Eur. Polym. J.* **2018**, *102*, 238.
- [87] Q. L. Feng, J. Wu, G. Q. Chen, F. Z. Cui, T. N. Kim, J. O. Kim, *J. Biomed. Mater. Res.* **2000**, *52*, 662.
- [88] J. T. Seil, T. J. Webster, *Int. J. Nanomed.* **2012**, *7*, 2767.
- [89] G. K. Auer, D. B. Weibel, *Biochemistry* **2017**, *56*, 3710.
- [90] T. L. A. Montanheiro, F. H. Cristóvan, J. P. B. Machado, et al., *J. Mater. Res.* **2014**, *30*, 55.
- [91] T. L. d. A. Montanheiro, L. S. Montagna, V. Patrulea, et al., *Polym. Test* **2019**, *79*, 106079.
- [92] D. T. Castro, R. D. Holtz, O. L. Alves, et al., *J. Appl. Oral Sci.* **2014**, *22*, 442.
- [93] R. D. Holtz, B. A. Lima, A. G. Souza Filho, et al., *Nanomed. Nanotechnol., Biol. Med.* **2012**, *8*, 935.
- [94] F. Barras, L. Aussel, B. Ezraty, *Antibiotics.* **2018**, *7*, 79.

**How to cite this article:** de Menezes BRC, Montanheiro TLdA, Sampaio AdG, Koga-Ito CY, Thim GP, Montagna LS. PCL/ $\beta$ -AgVO<sub>3</sub> nanocomposites obtained by solvent casting as potential antimicrobial biomaterials. *J Appl Polym Sci.* 2020;e50130. <https://doi.org/10.1002/app.50130>